processes

MDPI

Article

Selective Adsorption of Uranium from High Acid and High Chloride Zirconium Leach Liquor

Zhiping Yang [1,*], Haisheng Hu [1], Xiumin Jia [1] and Absai Vatuva [2]

[1] China-Namibia Joint Laboratory on Efficient Utilization of Uranium, Beijing Research Institute of Chemical Engineering and Metallurgy, Beijing 101149, China
[2] Department of Geosciences, University of Namibia, Gordon Street, Krönlein, Keetmanshoop 23001, Namibia
* Correspondence: yangzp@cnnc.com.cn

Abstract

Uranium associated with zircon sand enters zirconium leach liquor during acid leaching and can subsequently migrate into downstream process streams. Its direct recovery from industrial leach liquor is challenging because of the high acidity, chloride concentration, and low U/Fe ratio. Here, a macroporous chelating anion-exchange resin (CU600) was evaluated for direct uranium recovery without neutralization, dilution, or Fe pre-reduction. CU600 achieved a batch uranium adsorption capacity of 7.5 g U/L wet resin and a removal efficiency of 42.3%, approximately 2.1 times those of D201. Laboratory dynamic loadings were 21.2 and 18.6 g U/L wet resin, while the on-site loading reached 20.9 g U/L wet resin. Despite feed U/Fe mass ratios of approximately 0.1, the loaded-resin U/Fe ratio exceeded 0.8. Reductive iron stripping removed 42.8% of co-loaded Fe with 6.8% U loss, increasing the resin-phase U/Fe ratio from 0.879 to 1.43. Subsequent water elution produced peak uranium concentrations of 30.4 g/L in the laboratory and 17.5 g/L on site. These results support a process route integrating direct adsorption, selective iron stripping, and water elution, which enriches uranium into a concentrated eluate from industrial zirconium leach liquor.

Keywords: zirconium leach liquor; uranium recovery; selective adsorption; U–Fe separation

1. Introduction

Zircon sand ($ZrSiO_4$) is an important raw material for zirconium chemicals such as zirconium oxychloride. Its industrial hydrometallurgical route typically includes alkali decomposition, water leaching, acid leaching, concentration, and crystallization [1]. Natural zircon sand may contain associated uranium, thorium, and their decay products; consequently, the migration and accumulation of naturally occurring radioactive nuclides during zircon mineral processing are relevant to radiation protection and cleaner production [2,3]. Recent work on low-level zirconium oxychloride production has also linked hydrometallurgical operations such as acid leaching and crystallization with the control of radioactive impurities [4]. Selective recovery of associated uranium at the front end of the zirconium flowsheet could therefore reduce its transfer into downstream products, waste acid, and solid by-products while producing a uranium-enriched stream for subsequent recovery.

Previous studies have demonstrated the feasibility of uranium recovery from zirconium oxychloride-related streams. For example, Zhong and Wu treated zirconium oxychloride crystallization waste liquor by solvent extraction and investigated the separation of Fe, U, and Th in a highly acidic chloride medium, achieving high U recovery [5]. These results confirm that uranium in chloride systems of the zirconium industry can be recovered; however,

Check for updates

Academic Editor: Sebastien Farnaud

Received: 14 October 2026
Revised: 16 November 2026
Accepted: 23 November 2026
Published: 27 November 2026

Copyright: © 2026 by the authors. Licensee MDPI, Basel, Switzerland. This article is an open access article distributed under the terms and conditions of the Creative Commons Attribution (CC BY) license.

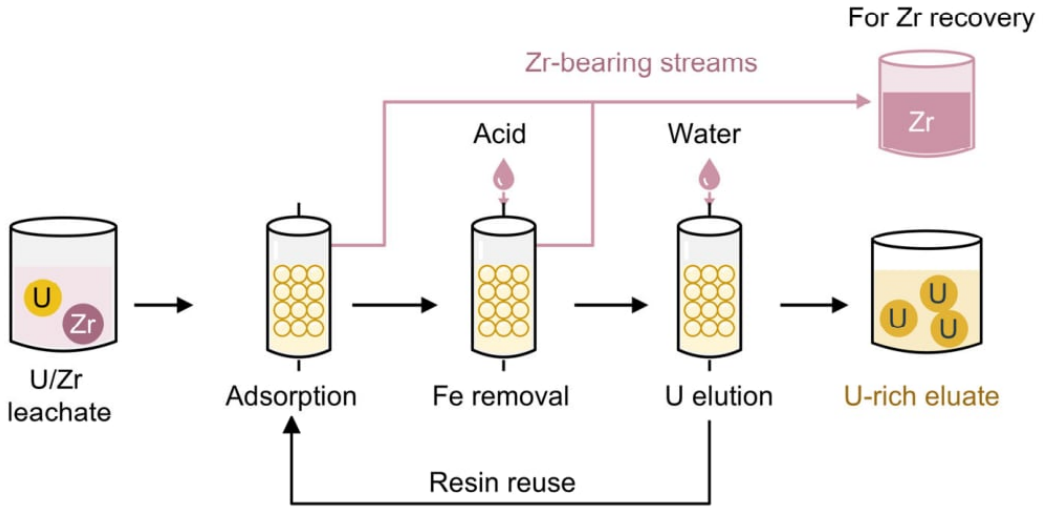
existing studies have focused mainly on downstream streams such as crystallization waste liquor. Moving the recovery step upstream to the zirconium leach liquor obtained after acid leaching would allow uranium to be intercepted before it enters subsequent concentration, crystallization, and waste-liquor systems, which is advantageous for reducing radionuclide migration among multiple process streams [6]. Nevertheless, published studies on the direct selective adsorption of uranium from real zirconium leach liquors remain limited.

Real zirconium leach liquors differ substantially from conventional low-salinity uranium-bearing aqueous systems. The liquor used in this study is characterized by high acidity and high concentrations of Cl^- and Fe, whereas U is present only at tens of milligrams per liter. In high-chloride media, the Cl^- concentration can markedly affect the aqueous speciation of U(VI) and its separation behavior; extraction and ion-exchange studies have shown that changes in Cl^- concentration can alter both the coordination environment of U(VI) and the adsorbed species in the resin phase [7,8]. In addition, uranium adsorption by anion-exchange resins is highly sensitive to the anionic composition of the medium, and sulfate, chloride, and nitrate systems can exhibit markedly different adsorption behavior [9].

Ion exchange and chelating adsorption are advantageous for enriching dilute uranium because they require simple equipment, can be operated continuously, and can produce a small-volume enriched solution during regeneration. Gonzalez-Luque and Streat systematically studied the adsorption and desorption of uranium by selective ion-exchange resins in phosphoric acid media and reported that coexisting ions such as Fe significantly reduce the effective resin capacity [10]. Kabay et al. further compared the uranium adsorption and desorption performance of several chelating ion-exchange resins in phosphoric acid systems and showed that the functional-group type, impurity competition, and regeneration performance jointly determine process applicability [11]. Furthermore, nitrogen-containing and chelating adsorbents have been widely used for the selective enrichment of uranium [12,13]. For polyamine/weak-base anion-exchange resins, coexisting Cl^- and Fe can also affect U extraction and impurity co-loading; therefore, selectivity evaluation should consider both U loading and the behavior of competing ions [14]. These studies indicate that, for complex industrial liquors, evaluation criteria should not be limited to equilibrium adsorption capacity but should also include competitive selectivity, dynamic breakthrough, impurity co-loading, and separation during regeneration.

In this system, Fe is the key coexisting impurity affecting the purity of the U product and the cycling performance of the resin. Because the Fe concentration in the feed is approximately one order of magnitude higher than that of U, even limited Fe co-adsorption can produce a resin loading comparable to or even higher than that of U, despite the high affinity of the resin for U. Therefore, rather than maximizing U loading alone, the more critical issue is whether the resin can substantially increase the resin-phase U/Fe ratio under a low feed U/Fe ratio and then preferentially remove co-loaded Fe during regeneration. Previous fixed-bed studies on U(VI) have shown that the feed concentration, flow rate, and bed height all affect breakthrough behavior, dynamic capacity, and bed utilization [15,16]. Consequently, dynamic breakthrough tests, washing/elution, and on-site-scale validation with real liquor are essential for assessing the scale-up potential of this process. The selection of CU600 for this position follows from the speciation of uranium in the feed and from a direct comparison with a conventional strong-base resin. In high-chloride solution U(VI) is present predominantly as $UO_2Cl_3^-$ and $UO_2Cl_4^{2-}$, which interact with the nitrogen-containing amine groups of CU600 through a combination of anion exchange and chelation, while the macroporous structure favors intraparticle mass transfer. Against the gel-type strong-base resin D201, CU600 gave a batch capacity of 7.5 versus 3.5 g U/L wet resin and a removal efficiency of 42.3% versus 19.7%, and broke through markedly later in the on-site column.

On this basis, the macroporous chelating anion-exchange resin CU600, whose specified functional group is amine, was evaluated for direct treatment of real high-acid, high-chloride zirconium leach liquor without neutralization, dilution, or Fe pre-reduction. Batch screening, laboratory fixed-bed breakthrough tests, competitive U–Fe loading, washing and water elution, reductive iron stripping in a sulfurous-acid (H_2SO_3) system, and on-site dynamic adsorption tests were used to evaluate three process-relevant aspects: dynamic U enrichment in a real complex liquor, U/Fe selectivity at feed U/Fe ratios of approximately 0.09–0.11, and preferential removal of co-loaded Fe. The objective was to assess the feasibility of moving associated-U recovery upstream to the zirconium leach-liquor stage and to provide a basis for a continuous process combining selective adsorption, iron stripping, and concentrated U elution. Scheme 1 summarizes the overall workflow of this study.



Scheme 1. The graphical abstract for U recovery from zirconium leach liquor using CU600.

2. Materials and Methods

2.1. Leach Liquor and Resin

The zirconium leach liquor was collected from the acid-leaching stage of an industrial wet-process zirconium oxychloride production line at a zirconium processing plant in southern China. The liquor composition varied slightly among batches; the compositions used for the laboratory and on-site tests are summarized in Table 1. Before adsorption, the liquor was subjected only to the cooling and clarification required for stable column operation. No neutralization, dilution, or chemical pre-reduction of Fe was performed. The CU600 used for adsorption is a macroporous chelating anion-exchange resin containing amine functional groups. CU600 was supplied by Hebi Hairuige Technology Co., Ltd. (Hebi, Henan Province, China), and the reference resin D201 was supplied by Zhejiang Zhengguang Industrial Co., Ltd. (Hangzhou, Zhejiang Province, China). Table 2 summarizes the main technical parameters of CU600 and D201.

Table 1. Main composition of the laboratory and on-site zirconium leach liquors.

Batch	U ($mg\ L^{-1}$)	TFe ($mg\ L^{-1}$)	Fe^{3+} ($mg\ L^{-1}$)	Th ($mg\ L^{-1}$)	Ti ($mg\ L^{-1}$)	Cl^- ($g\ L^{-1}$)	PO_4^{3-} ($mg\ L^{-1}$)	H^+ ($mol\ L^{-1}$)	ZrO_2 ($g\ L^{-1}$)	U/Fe
Laboratory liquor	71	612	581	55	190	181.9	65	2.76	105.6	0.116
On-site liquor	64	710	675	49	178	180.8	76	2.9–3.5	105	0.090

Note: TFe represents total iron concentration. The measurements for TFe were performed by ICP-MS.

Table 2. Main technical parameters of the CU600 and D201 resin.

Property	CU600	D201
Appearance	White spherical beads	Milky white to pale yellow opaque spherical beads
Functional group	Nitrogen-containing heterocyclic amine chelating groups	Quaternary ammonium groups
Water content (%)	57–62	50.00–60.00
Wet apparent density (g mL^{-1})	0.60–0.70	0.65–0.73
Particle size range (mm)	0.40–1.25 (≥95%)	0.315–1.250 (≥95%)
Total exchange capacity (mmol g^{-1})	3.4	3.7
Bed void volume (%)	40	40
Ionic form as supplied	Chloride form (Cl^-)	Chloride form (Cl^-)

2.2. Resin Pretreatment and Adsorption Tests

All solutions were prepared with laboratory deionized water (conductivity below 0.10 mS/m at 25 °C). Before use, the resin was conditioned sequentially. The resin was first contacted with 8 bed volumes (BV) of 1 mol/L NaOH for 30 min and then soaked in 8 BV of deionized water for 30 min. It was subsequently acidified with 8 BV of 1 mol/L hydrochloric acid (HCl) for 30 min. Finally, the resin was rinsed with deionized water at 25–30 mL/min for 30 min until the effluent was approximately neutral. One physical bed volume corresponds to the settled wet-resin volume, V_r.

For each batch test, 2.0 mL of wet CU600 or D201 resin was contacted with 500 mL of laboratory zirconium leach liquor at room temperature for 5 h. After adsorption, the residual uranium concentration was measured. The uranium removal efficiency, R, and the wet-volume-based adsorption capacity, q, were calculated using Equations (1) and (2):

$$R = (C_0 - C_e)/C_0 \times 100\% \quad (1)$$

$$q = (C_0 - C_e)V/(1000V_r) \quad (2)$$

where C_0 and C_e are the initial and final uranium concentrations in solution (mg/L), respectively; V is the solution volume (mL); and V_r is the wet-resin volume (mL). With these units, q is expressed in g U/L wet resin. C_e denotes the concentration measured after the specified 5 h contact period.

In the laboratory dynamic tests, 50 mL of CU600 was packed into the column, giving a resin bed height of about 600 mm and a recorded contact time of 4 min; the field test used 250 mL of CU600, a bed height of about 800 mm and a recorded contact time of 5 min. A separate series of laboratory fixed-bed tests was run on the same bed and the same liquor at contact times of 3, 5, 10 and 20 min, each followed to about 560 BV; because the bed was unchanged, the contact time is inversely proportional to the flow rate. The dynamic loading was calculated by accumulating the difference in uranium mass between the inlet and outlet of each fraction. All dynamic runs were terminated before complete bed saturation, the outlet uranium concentration remaining below the feed concentration at the end of every run, so that the values reported here are the dynamic loadings at run termination rather than the maximum dynamic adsorption capacity of the bed.

After dynamic adsorption, the resin bed was first washed with a 3.5 mol/L HCl solution, and uranium was then eluted with water in fractions. The elution ratio was calculated as the ratio of the sum of the uranium mass in the wash and eluate solutions to the mass of uranium adsorbed on the resin. The reductive iron stripping test used a sulfurous-acid system; 43 mL of loaded resin contained 1.23 g of U and 1.40 g of Fe, and the stripping solution, consisting of 90 mL of 6% H_2SO_3, 150 mL of 12 mol/L HCl (approximately 3.5 BV) and 210 mL of water, was passed through the resin in two stages.

2.3. Characterization

The concentrations of U, Fe, and other elements in feed, raffinate, wash, stripping, and eluate solutions were determined by inductively coupled plasma mass spectrometry (ICP-MS; iCAP RQ, Thermo Fisher Scientific, Waltham, MA, USA). The method was evaluated at several concentration levels covering the range of the measured samples, and the within-laboratory relative standard deviation ranges from 2.3% to 11.2% and narrows as the concentration increases, with good repeatability and reproducibility. The description of the analytical method has been refined accordingly, and the reliability of the measured results is supported by the precision of the method. Fourier-transform infrared (FTIR) spectra of pristine and uranium-loaded CU600 were recorded using a TENSOR II spectrometer (Bruker, Ettlingen, Germany) to compare changes in the chemical environment of the resin functional groups before and after uranium adsorption.

3. Results and Discussion

3.1. Batch Adsorption Performance

In the laboratory high-acid, high-chloride liquor, the U concentration of the raffinate after adsorption on CU600 was 41 mg/L, corresponding to an adsorbed amount of 15 mg, a batch adsorption capacity of 7.5 g U/L wet resin, and a removal efficiency of 42.3%. For D201, the U concentration of the raffinate was 57 mg/L, corresponding to an adsorption capacity of 3.5 g U/L wet resin and a removal efficiency of 19.7%. Under identical liquor composition, resin volume, and contact time, the U adsorption capacity and removal efficiency of CU600 were both approximately 2.1 times those of D201 (Figure 1). This difference cannot be attributed solely to the total exchange capacity of the resins. In high-chloride, high-acid media, the chloride complexation of U and Fe, Cl^- competition, and amine protonation all affect the available adsorption sites and mass-transfer process [17]. The higher apparent adsorption performance of CU600 may therefore result from the combined contributions of functional-group accessibility, intraparticle mass transfer, and complexation/ion-exchange interactions. Previous studies have shown that the pore structure of a resin can significantly affect the mass transfer and adsorption rate of U [18].

The adsorption capacity of CU600 increased rapidly during the first 3 h and gradually approached a plateau at 5 h (Figure 2). As the temperature increased from 20 to 40 °C, the adsorption capacity at 5 h increased from 7.50 to 8.40 g U/L wet resin. The pseudo-second-order model provided better fitting results than the pseudo-first-order model, with the rate constant and initial adsorption rate increasing with temperature (Table 3). The Weber–Morris model also showed good linearity. These results suggest that uranium adsorption on CU600 involves both interactions between uranium chloro complexes and nitrogen-containing functional groups and mass transfer within the resin pores.

Table 3. Kinetic parameters of uranium adsorption on CU600 at different temperatures.

Kinetic Model	Parameter	20 °C	30 °C	40 °C
Pseudo-first-order	q_e (g U L^{-1} wet resin)	7.338	7.613	7.932
	k_1 (h^{-1})	0.7187	0.9122	1.0229
	R^2	0.951	0.914	0.925
Pseudo-second-order	q_e (g U L^{-1} wet resin)	9.291	9.266	9.517
	k_2 (L g^{-1} h^{-1})	0.0774	0.1084	0.1221
	h_0 (g U L^{-1} h^{-1})	6.68	9.30	11.06
	R^2	0.980	0.966	0.977

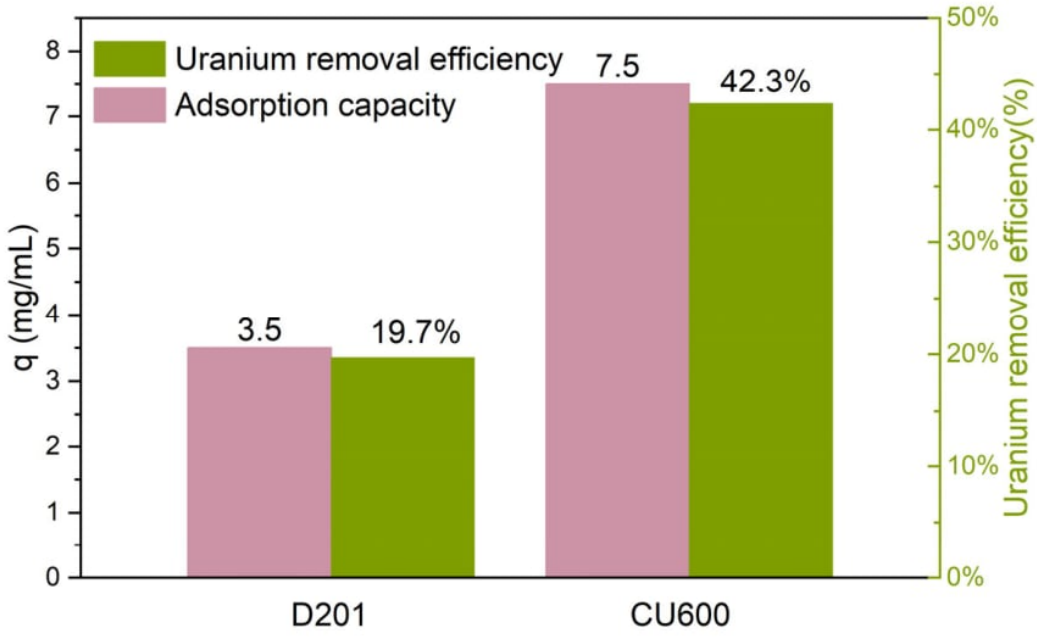


Figure 1. Batch uranium adsorption capacity and uranium removal efficiency of CU600 and D201 resins in high-acid, high-chloride zirconium leach liquor; Both resins were tested under identical liquor composition, resin volume and contact time.

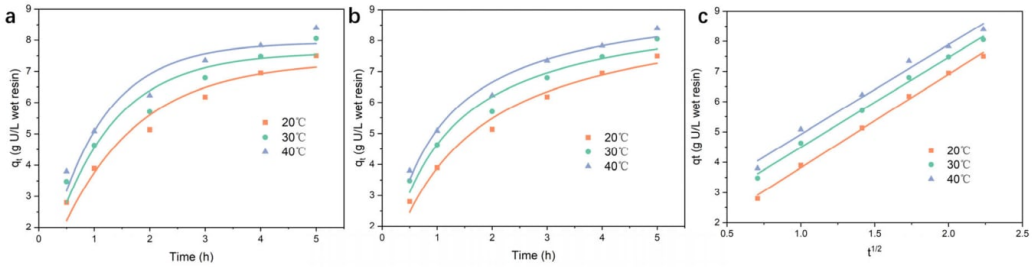


Figure 2. Kinetic fitting of uranium adsorption on CU600 at 20 °C, 30 °C, and 40 °C: (**a**) pseudo-first-order model, (**b**) pseudo-second-order model, and (**c**) Weber–Morris intra-particle diffusion model.

3.2. Laboratory Dynamic Adsorption Performance

In the first dynamic adsorption run, 50 mL of CU600 treated 23.8 L (476 BV) of liquor and adsorbed a cumulative 1061.7 mg of U, corresponding to a dynamic loading of 21.2 g U/L wet resin. As shown in Figure 3a, the outlet U concentration increased gradually over approximately 100–300 BV and then rose more slowly, indicating that the mass-transfer zone had advanced toward the bed outlet; however, the outlet concentration remained below the feed concentration at the end of the run. The second run treated 27.95 L (559 BV) of liquor and adsorbed 931.4 mg of U, corresponding to a dynamic loading of 18.6 g U/L wet resin. In Figure 3b, the normalized outlet U concentration increased continuously after approximately 200 BV and approached 0.8 at approximately 500 BV. The similar dynamic loadings obtained in the two runs indicate that CU600 has a relatively stable dynamic U enrichment capacity in this real high-acid, high-chloride system.

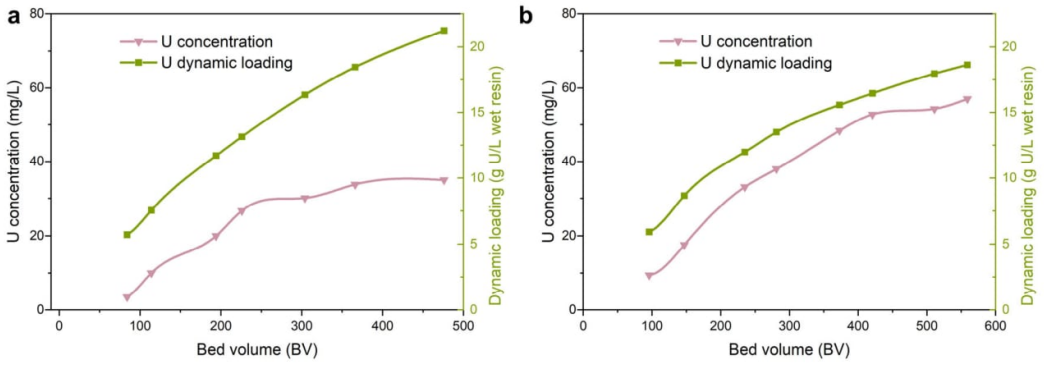


Figure 3. Uranium breakthrough curves and dynamic loadings of the laboratory dynamic adsorption tests: (**a**) first run; (**b**) second run.

Figure 4 shows the effect of contact time on uranium breakthrough behavior. The effluent uranium concentration increased with bed volume at all contact times. Shorter contact times resulted in earlier breakthrough and higher effluent uranium concentrations. At approximately 560 BV, the effluent uranium concentration decreased from 57.0 mg/L at 3 min to 32.7 mg/L at 20 min, while the dynamic loading increased from 20.7 to 29.5 g U/L wet resin. The breakthrough curves at 10 and 20 min were similar, indicating that a contact time of approximately 10 min was sufficient for adequate mass transfer. These results suggest that longer contact times improve uranium uptake by reducing the limitations associated with film diffusion and intraparticle mass transfer.

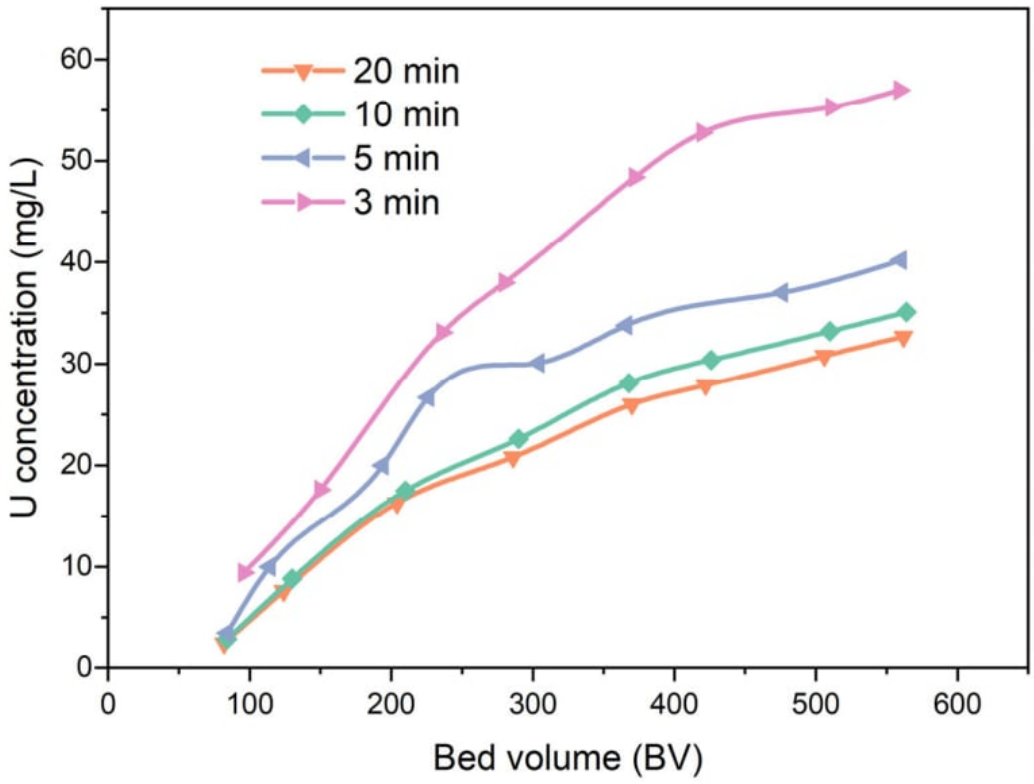


Figure 4. Effect of contact time on uranium breakthrough behavior of CU600 resin in high-acid, high-chloride zirconium leach liquor.

3.3. Selective U–Fe Adsorption Under High Loading

The loaded resin from the second run contained 17.0 g U/L wet resin and 21.2 g Fe/L wet resin, corresponding to a U/Fe mass ratio of 0.802. In the third run, after the feed U

concentration was increased to 122 mg/L (Figure 5a), the U and Fe loadings increased to 28.6 g U/L and 32.6 g/L, respectively, and the U/Fe mass ratio reached 0.877 (Figure 5b). Relative to the feed liquor, this compositional change more directly reflects the competitive selectivity of CU600: the U/Fe ratios of the laboratory and on-site feed liquors were 0.116 and 0.090, respectively, whereas the U/Fe ratio of the loaded resin reached 0.802 and 0.877, This substantial increase in the resin-phase U/Fe ratio indicates the preferential enrichment of uranium over iron during the adsorption process. Thus, despite the Fe mass concentration in the feed being approximately 10 times higher than the U concentration, the two metals reached nearly equal mass loadings in the resin phase. This result demonstrates the pronounced competitive adsorption advantage of CU600 for U. When the feed U concentration was further increased, the U loading increased by approximately 68%, while the U/Fe ratio rose from 0.802 to 0.877. These changes indicate that higher U loading further improves the U–Fe composition of the resin phase.

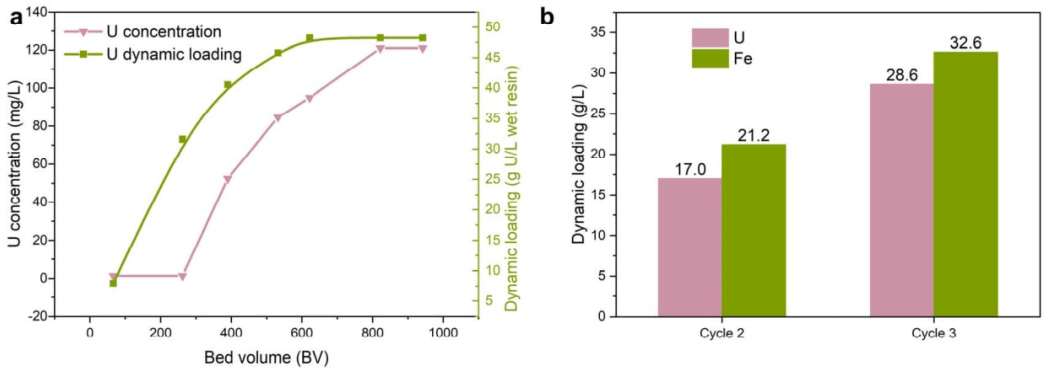


Figure 5. Competitive U–Fe adsorption under high loading: (**a**) uranium breakthrough curve and dynamic loading of the third run (feed U concentration of 122 mg/L); (**b**) solid-phase U and Fe loadings of the loaded resins from the second and third runs.

3.4. Characterization of CU600 Before and After Uranium Adsorption

Figure 6 shows the N_2 adsorption–desorption isotherm of the pristine CU600 resin. The adsorption amount increased gradually at low and intermediate relative pressures, followed by a sharp increase at high relative pressure ($P/P0 > 0.9$), accompanied by a hysteresis loop. This behavior suggests the presence of mesopore-type porosity. The BET specific surface area of CU600 was 10.21 m^2/g. These results indicate that CU600 possesses a porous structure that may facilitate solution transport and intraparticle mass transfer during uranium adsorption. The internal pore structure was further examined by cross-sectional SEM.

Figure 7 shows the cross-sectional SEM images of CU600 before and after uranium adsorption. At higher magnification, interconnected channels formed by aggregated particles were observed within the resin. After uranium loading, the cross-sectional morphology and internal channels were largely retained, indicating that the porous structure remained stable during adsorption. These channels may facilitate solution penetration and intraparticle mass transfer, contributing to uranium uptake by CU600.

EDS elemental mapping (Figure 8) revealed the distribution of U, Fe, C, and N in CU600 before and after uranium adsorption. After uranium loading, U signals were observed throughout the resin cross-section, indicating that uranium entered the bead interior rather than remaining confined to the outer surface. These results, together with the BET and SEM observations, suggest that the internal porous structure of CU600 provides pathways for uranium transport and adsorption.

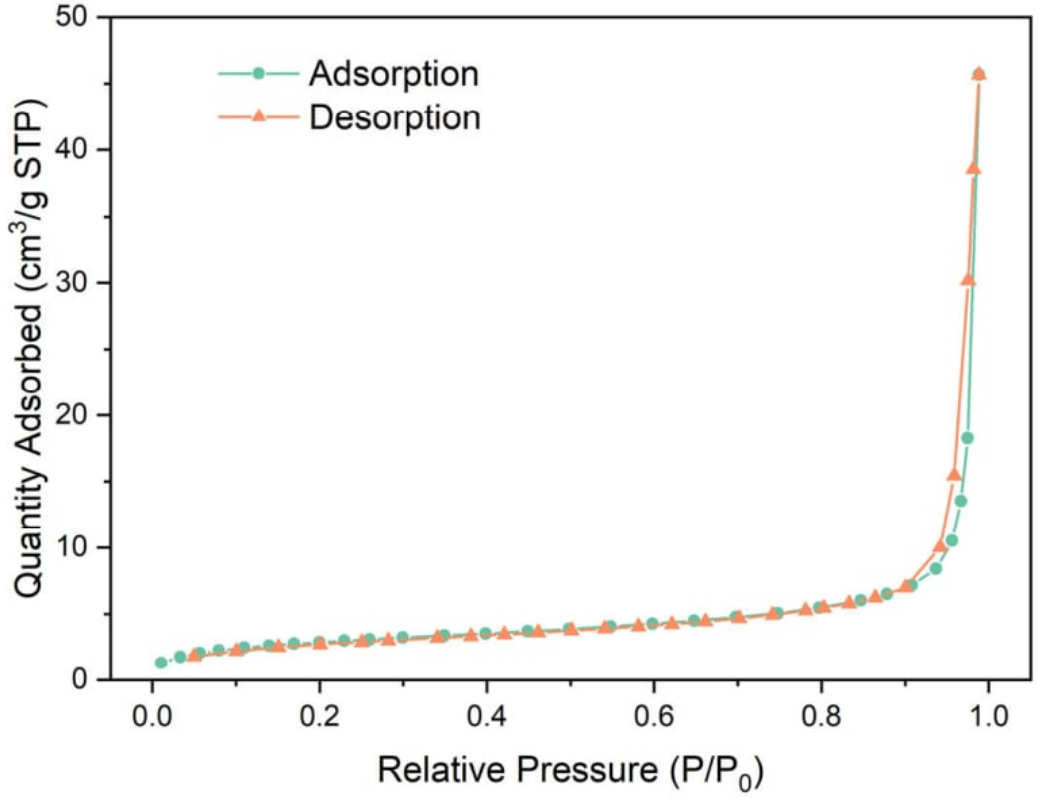


Figure 6. N_2 adsorption–desorption isotherm of the pristine CU600 resin.

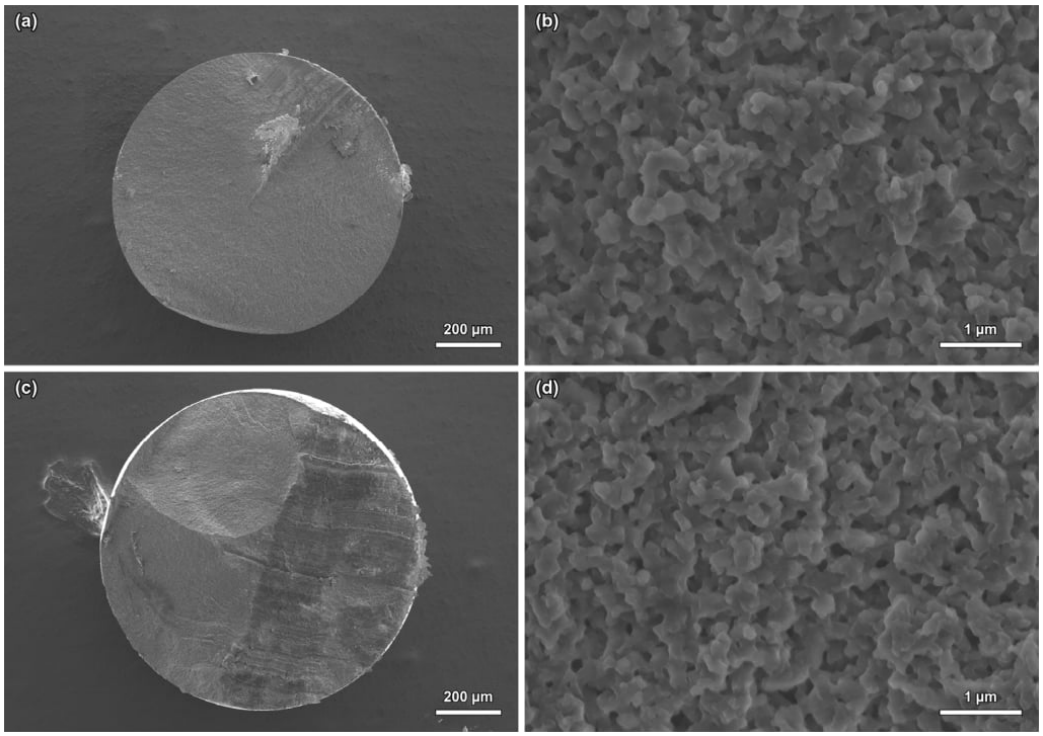


Figure 7. Cross-sectional SEM images of pristine (**a**,**b**) and U-loaded (**c**,**d**) CU600 resin.

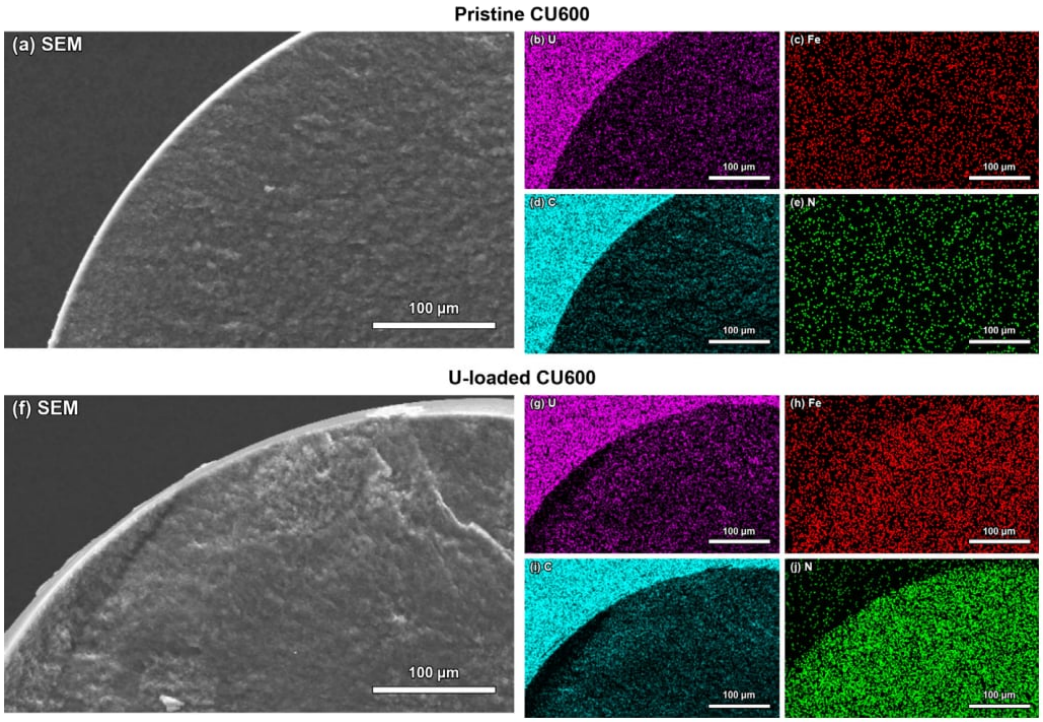


Figure 8. Cross-sectional SEM images (**a**,**f**) and EDS elemental maps of U (**b**,**g**), Fe (**c**,**h**), C (**d**,**i**), and N (**e**,**j**) for pristine (**a**–**e**) and U-loaded (**f**–**j**) CU600 resin.

To examine changes in the chemical environment of CU600 before and after uranium adsorption, pristine and uranium-loaded resins were characterized by Fourier-transform infrared spectroscopy (FTIR; Figure 9). The pristine resin showed a broad band near 3400 cm^{-1}, mainly from N-H stretching of the protonated piperidine amine groups. Bands at 1600–1400 cm^{-1} were assigned to the aromatic C=C skeletal stretching of the polystyrene matrix, while those at 1200–800 cm^{-1} corresponded to C-N stretching vibrations of the piperidine ring and C-H in-plane bending of the aromatic rings.

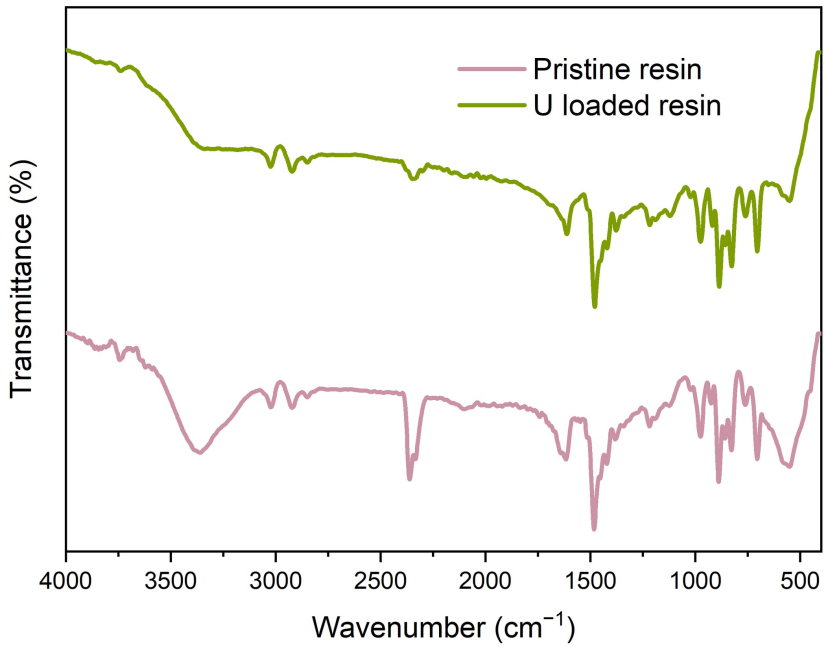


Figure 9. FTIR spectra of the pristine and uranium-loaded CU600 resins.

After uranium loading the peak shape and relative intensity changed markedly; the N-H stretching band at 3400 cm^{-1} significantly decreased or nearly disappeared and the C-N band near 1146 cm^{-1} red-shifted indicating that the piperidine nitrogen atoms strongly coordinate with U(VI) and act as the primary binding sites thereby weakening or eliminating the N-H vibrational feature [19,20]. These spectral changes suggest that the chemical environment of the nitrogen-containing functional groups was altered after uranium uptake, indicating their possible involvement in U(VI) adsorption [21].

3.5. Washing, Water Elution, and Uranium Enrichment

After the loaded resin from the first run was washed with 400 mL of 3.5 mol/L HCl, 148 mg of U was detected in the acid-wash solution. The U concentration in the first 45 mL water-eluate fraction reached 16.6 g/L, whereas that in the following 250 mL fraction decreased to 0.4 g/L. The acid wash displaced the process liquor retained in the bed and also removed part of the resin-associated U. Subsequent reduction in acidity and ionic strength changed the conditions governing U(VI) speciation and resin–U interactions, favoring desorption; enhanced U(VI) desorption from anion-exchange resins at lower acidity has also been reported [22]. The resulting concentrated elution peak shows that resin-phase U can be transferred into a comparatively small volume of eluate.

During the second water-elution test (Figure 10b), the U and Fe concentrations in the third eluate fraction (25 mL) reached 30.4 and 24.0 g/L, respectively, and then decreased rapidly. Water elution therefore produced a concentrated U peak, but co-loaded Fe was released simultaneously. To further reduce the purification cost of the uranium-bearing intermediate eluate, it is of great research significance to investigate the selective stripping of Fe from the loaded resin.

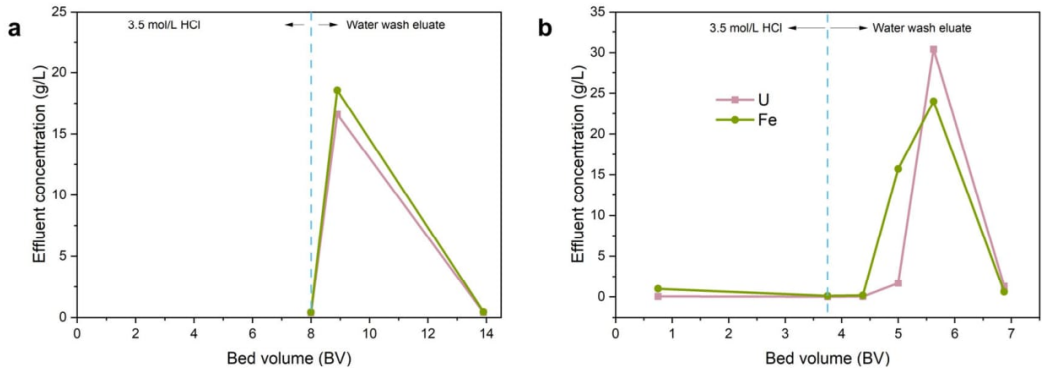


Figure 10. Acid washing and water elution curves of the laboratory dynamic adsorption tests: (**a**) U concentration of the effluent in the first run; (**b**) uranium and Fe concentrations of the effluent in the second run. The dashed line marks the boundary between the washing stage and the water elution stage.

3.6. Reductive Iron Stripping and U–Fe Separation

The results of dynamic iron stripping are summarized in Table 4. The first and second stripping fractions eluted 0.28 and 0.32 g of Fe, respectively, for a total Fe removal of 0.60 g, equivalent to 42.8% of the initially loaded Fe (1.40 g). Over the same period, 0.084 g of U was eluted, corresponding to 6.8% of the initially loaded U (1.23 g). The resin-phase U/Fe mass ratio before stripping was 0.879. After stripping, approximately 1.146 g of U and 0.80 g of Fe remained on the resin, increasing the resin-phase U/Fe mass ratio to approximately 1.43. Thus, under the tested conditions, the sulfurous-acid system preferentially removed co-loaded Fe relative to U.

Table 4. Results of dynamic iron stripping with the sulfurous-acid system.

Stripping Fraction	Volume (mL)	U Concentration (mg L^{-1})	Fe Concentration (g L^{-1})	U Eluted (g)	Fe Eluted (g)
Iron stripping 1	140	216	2.00	0.030	0.28
Iron stripping 2	305	177	1.05	0.054	0.32
Total/proportion				0.084 (6.8%)	0.60 (42.8%)

3.7. On-Site Verification of Dynamic Adsorption

The on-site dynamic adsorption test used 250 mL of wet CU600 resin. As shown in Figure 11a, the outlet U concentration was 0.52 mg/L after 5 L of liquor had been treated. At 48 BV, adjacent outlet measurements were approximately 0.84 mg/L; accordingly, approximately 48 BV was used as the operational early-breakthrough point. Thereafter, the outlet U concentration increased gradually but remained below the feed concentration over the measured range. After 162.3 L had been treated, the outlet U concentration was 39.9 mg/L, approximately 62% of the 64 mg/L feed concentration. The cumulative adsorbed U was 5221 mg, corresponding to a dynamic loading of 20.9 g U/L wet resin. D201 showed earlier breakthrough: its outlet U concentration reached 2.8 mg/L after only 4.1 L (16.4 BV) and 59.9 mg/L after 138.9 L. At a comparable cumulative treated volume of approximately 32 L, the outlet U concentrations were 13.5 mg/L for CU600 and 43.4 mg/L for D201. These data show later breakthrough and lower outlet U concentrations for CU600 under the on-site test conditions. The schematic diagram of the on-site dynamic adsorption apparatus is shown in Figure 11b.

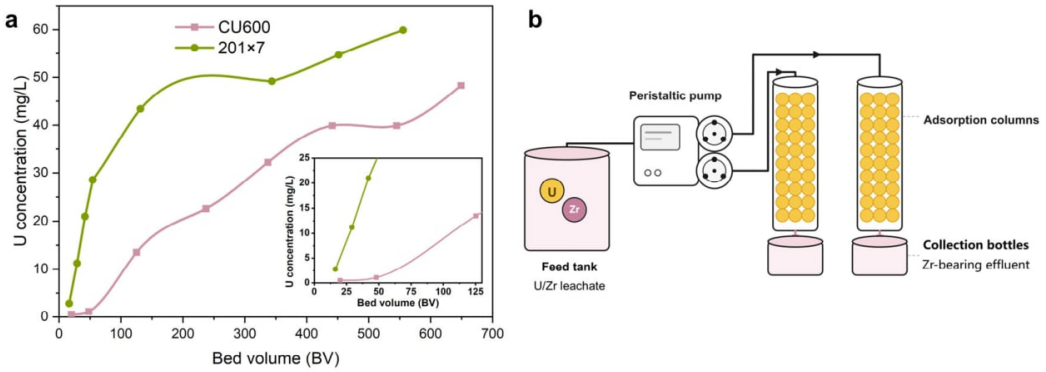


Figure 11. On-site dynamic adsorption performance: (**a**) uranium breakthrough curves of CU600 and D201 in the on-site zirconium leach liquor (inset: enlarged local view); (**b**) schematic diagram of the on-site adsorption unit.

The loaded CU600 from the on-site test was acid-washed and then eluted with water. As shown in Figure 12, during the acid washing stage (3.5 mol/L HCl), the effluent concentrations of both U and Fe were maintained at relatively low levels. Upon switching to the water elution stage, both concentrations increased sharply. The U concentrations in the third and fourth eluate fractions reached 16.0 and 17.5 g/L, respectively, showing that most of the eluted U was concentrated within a relatively small elution volume. By 4.0 BV, the concentrations of both elements had dropped back to relatively low levels. Compared with the laboratory profiles (Figure 10), the on-site peak was broader and lower. Differences in bed height, flow stability, liquor temperature, or packing uniformity may contribute to this behavior, although these factors were not varied independently in the present study. The first four eluate fractions recovered 91.6% of the U originally loaded on the column, confirming concentrated U recovery at the on-site scale.

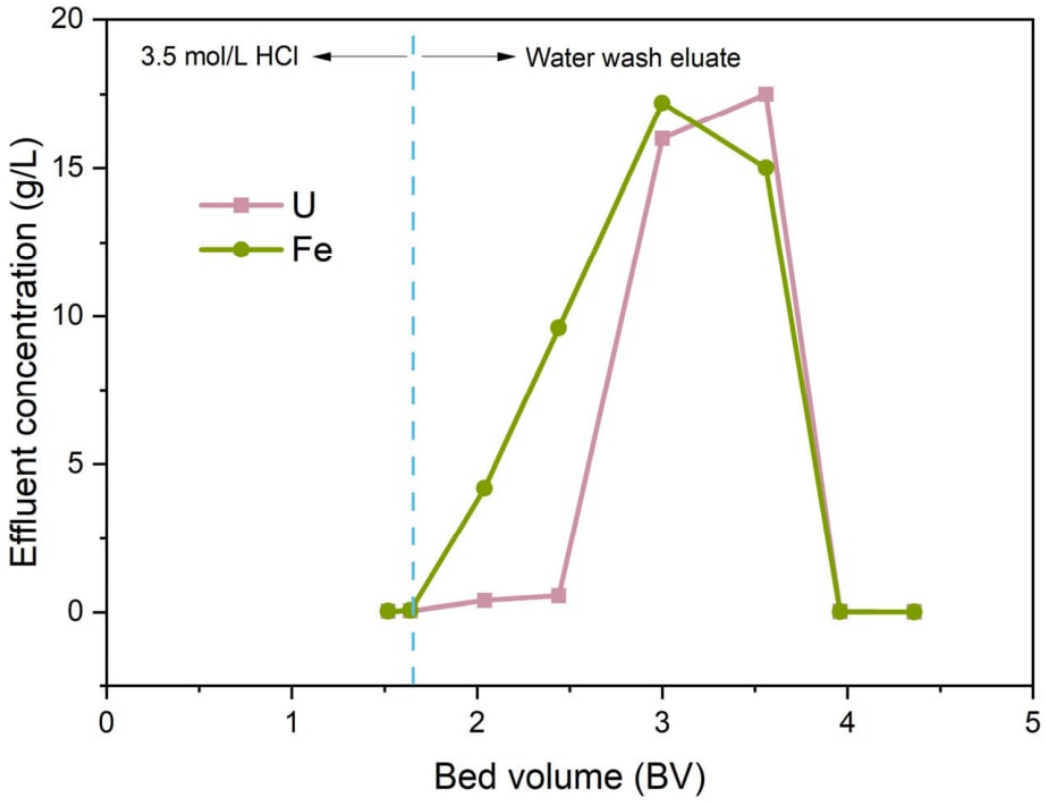


Figure 12. U concentration of the effluents from acid washing and water elution of the on-site fixed bed; the dashed line marks the boundary between the washing stage and the water elution stage.

Based on the laboratory and on-site validation results, a process route for uranium recovery from U-bearing zirconium leach liquor was developed, as illustrated in Figure 13. The feed liquor was first subjected to CU600 adsorption, where uranium was preferentially enriched over iron. The U/Fe mass ratios increased from 0.116 and 0.090 in the laboratory and on-site feed liquors to 0.802 and 0.877 in the corresponding loaded resins, respectively. Subsequently, the co-loaded iron was selectively removed through reductive stripping, followed by water elution to obtain a concentrated uranium solution. The adsorption raffinate can then return to the zirconium recovery circuit. After the target loading is reached, residual zirconium liquor is drained and the bed is washed; these streams can likewise be returned to the zirconium circuit to limit Zr loss. Co-loaded Fe is then preferentially stripped using the sulfurous-acid system. Under the tested conditions, this step removed 42.8% of Fe with 6.8% U loss and increased the resin-phase U/Fe ratio from approximately 0.88 to 1.43. Water elution subsequently transfers U into a small-volume enriched solution; in the on-site test, the first four water-eluate fractions recovered 91.6% of the U initially loaded on the column. The experimental results therefore support a sequence of selective adsorption, liquor recovery/washing, reductive Fe stripping, and concentrated U elution. Multi-cycle resin stability, the Fe-stripping end point, and crystallization control remain to be established in future engineering work.

The chemical compositions of the on-site uranium-bearing eluate and the resin sample after elution are presented in Table 5. The uranium and iron concentrations in the analyzed eluate were 17.5 and 19.6 g/L, respectively, corresponding to a U/Fe mass ratio of 0.89, approximately 9.9 times that of the original on-site leach liquor (0.090). The concentrations of Th, Ti, SiO_2, and $PO_4^{(3-)}$ were all below 1 mg/L, while the ZrO_2 concentration was 20.5 mg/L. In addition, the H^+ and Cl^- concentrations decreased to 0.2 mol/L and 13.8 g/L, respectively, substantially lower than those in the original leach liquor. These results

indicate that uranium was effectively enriched in the eluate while the concentrations of major zirconium-related matrix components were markedly reduced.

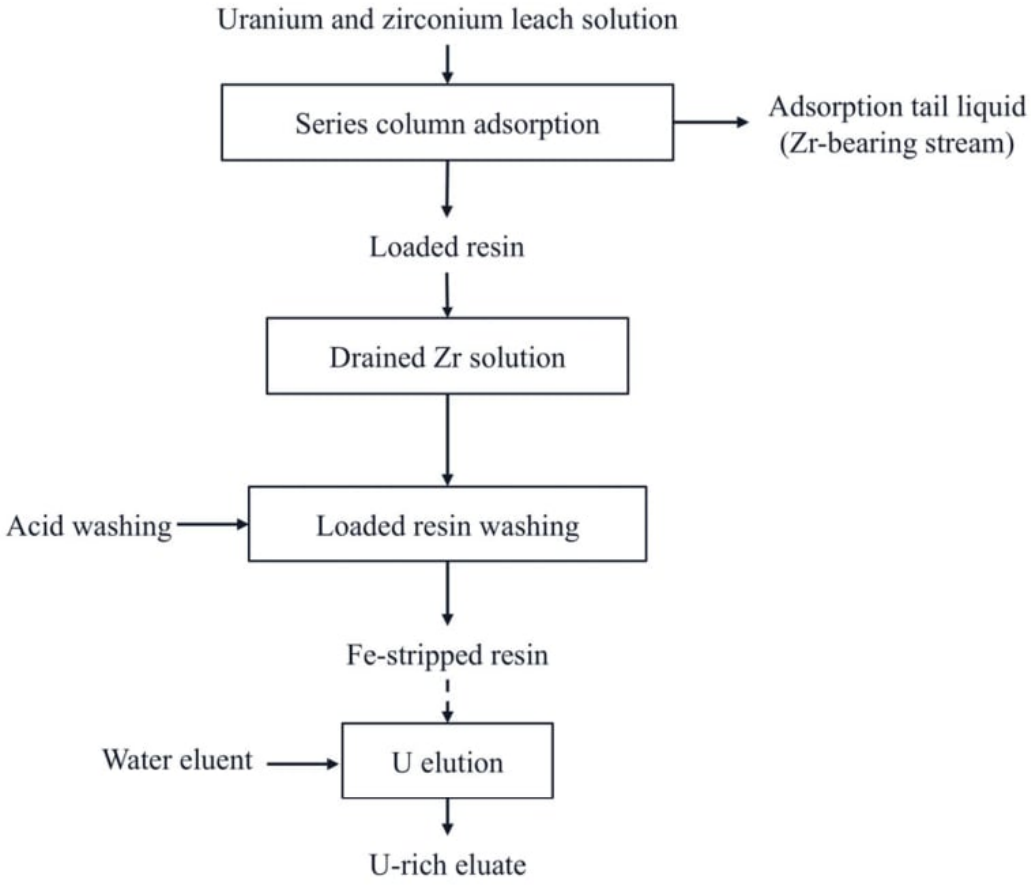


Figure 13. Proposed process flowsheet for direct fixed-bed U adsorption from zirconium leach liquor, liquor recovery and washing, reductive Fe stripping, water elution.

Table 5. Chemical composition of the on-site uranium-bearing eluate and resin after water elution.

On-Site Uranium-Bearing Eluate	U g L^{-1}	Th mg L^{-1}	Ti mg L^{-1}	SiO_2 mg L^{-1}	PO_4^{3-} mg L^{-1}	Fe g L^{-1}	Cl^- g L^{-1}	H^+ mol L^{-1}	ZrO_2 mg L^{-1}
U-bearing eluate	17.5	<1	<1	<1	<1	19.6	13.8	0.2	20.5
Stripped resin	0.038	<1	<1	36	41	16	-	-	35

4. Conclusions

This study demonstrated the feasibility of directly recovering uranium from real high-acid, high-chloride zirconium leach liquor using the macroporous chelating anion-exchange resin CU600 without neutralization, dilution, or Fe pre-reduction. CU600 exhibited superior uranium adsorption performance compared with D201, achieving a batch adsorption capacity of 7.5 g U/L wet resin and a uranium removal efficiency of 42.3%, both approximately 2.1 times higher than those of D201 under identical conditions. In fixed-bed adsorption experiments, CU600 maintained stable uranium enrichment performance, with dynamic loadings of 21.2 and 18.6 g U/L wet resin in laboratory-scale columns and 20.9 g U/L wet resin in the on-site validation test.

CU600 also exhibited effective U–Fe separation capability in the complex chloride-rich matrix. The feed liquors used in the laboratory and on-site experiments showed U/Fe mass ratios of 0.116 and 0.090, respectively, while the corresponding loaded resins

reached U/Fe mass ratios of 0.802 and 0.877, respectively. This improvement indicates that CU600 preferentially enriched uranium over iron during the adsorption process, despite the significantly higher iron concentration in the feed liquor. Furthermore, reductive iron stripping using a sulfurous-acid system selectively removed co-loaded Fe from the loaded resin, achieving 42.8% Fe removal with only 6.8% uranium loss and increasing the resin-phase U/Fe mass ratio from 0.879 to 1.43.

Subsequent water elution effectively recovered uranium into a concentrated eluate, producing maximum uranium concentrations of 30.4 g/L in laboratory experiments and 17.5 g/L in the on-site test. In the on-site elution experiment, the first four eluate fractions recovered 91.6% of the uranium initially loaded onto the column. Overall, these results validate a process strategy integrating selective adsorption, reductive Fe stripping, and concentrated water elution for uranium recovery from zirconium leach liquor. These results support the selective enrichment of uranium, preferential removal of co-loaded iron, and recovery of a uranium-enriched eluate as an intermediate stream for subsequent purification. Future work should evaluate multi-cycle resin stability, optimize iron stripping to minimize uranium loss, and assess eluate purification and stream recycling within the zirconium recovery circuit.

Author Contributions: Conceptualization, Z.Y. and X.J.; methodology, Z.Y.; software, H.H.; validation, H.H., and Z.Y.; formal analysis, Z.Y. and A.V.; investigation, Z.Y.; resources, X.J.; data curation, Z.Y.; writing—original draft preparation, Z.Y.; writing—review and editing, H.H., X.J. and A.V.; visualization, H.H.; supervision, Z.Y.; project administration, Z.Y.; funding acquisition, X.J. All authors have read and agreed to the published version of the manuscript.

Funding: This work was supported by National Key R&D Program of China [grant numbers: 2024YFE0213700].

Data Availability Statement: The original contributions presented in this study are included in the article. Further inquiries can be directed to the corresponding author.

Acknowledgments: During the revision process of this work, the lead author used Deepseek-V4.1 (DeepSeek, Hangzhou, China) in order to improve language and readability of some sentences. AI was not involved in the scientific research, data analysis, or writing of the original scientific content. All authors take full responsibility for the content.

Conflicts of Interest: The authors declare that they have no known competing financial interests or personal relationships that could have appeared to influence the work reported in this paper.

References

1. Song, J.; Fan, J.-F.; Liu, J.-C.; Liu, R.; Qu, J.-K.; Qi, T. A Two-Step Zircon Decomposition Method to Produce Zirconium Oxychloride: Alkali Fusion and Water Leaching. *Rare Met.* **2020**, *39*, 448–454. [CrossRef]
2. Ballesteros, L.; Zarza, I.; Ortiz, J.; Serradell, V. Occupational Exposure to Natural Radioactivity in a Zircon Sand Milling Plant. *J. Environ. Radioact.* **2008**, *99*, 1525–1529. [CrossRef] [PubMed]
3. Venkateswara Rao, C.; Rout, A.; Venkatesan, K.A. Selective Separation of Zirconium(IV) from Uranium(VI) Using Dioxoamide Ligand Present in Ammonium Based Ionic Liquid: An Application towards Spent Metallic Fuel Reprocessing. *Sep. Purif. Technol.* **2020**, *247*, 116963. [CrossRef]
4. Supriadi, H.; Poernomo, H.; Basuki, K.T.; Astuti, W.; Suyanti, S.; Handini, T.; Ayatillah, N.S.; Taftazani, A.; Prameswara, G. Characterization and Kinetics of Low-TENORM Zirconium Oxychloride Production from Zircon Sand. *Transit. Met. Chem.* **2025**, *50*, 241–251. [CrossRef]
5. Zhong, X.; Wu, Y. Recovery of Uranium and Thorium from Zirconium Oxychloride by Solvent Extraction. *J. Radioanal. Nucl. Chem.* **2012**, *292*, 355–360. [CrossRef]
6. Quinn, J.E.; Wilkins, D.; Soldenhoff, K.H. Solvent Extraction of Uranium from Saline Leach Liquors Using DEHPA/Alamine 336 Mixed Reagent. *Hydrometallurgy* **2013**, *134–135*, 74–79. [CrossRef]
7. Quinn, J.E.; Ogden, M.D.; Soldenhoff, K. Solvent Extraction of Uranium (VI) from Chloride Solutions Using Cyphos IL-101. *Solvent Extr. Ion. Exch.* **2013**, *31*, 538–549. [CrossRef]

8. Moon, E.M.; Ogden, M.D.; Griffith, C.S.; Wilson, A.; Mata, J.P. Impact of Chloride on Uranium(VI) Speciation in Acidic Sulfate Ion Exchange Systems: Towards Seawater-Tolerant Mineral Processing Circuits. *J. Ind. Eng. Chem.* **2017**, *51*, 255–263. [CrossRef]
9. Zagorodnyaya, A.N.; Abisheva, Z.S.; Sharipova, A.S.; Sadykanova, S.E.; Bochevskaya, Y.G.; Atanova, O.V. Sorption of Rhenium and Uranium by Strong Base Anion Exchange Resin from Solutions with Different Anion Compositions. *Hydrometallurgy* **2013**, *131–132*, 127–132. [CrossRef]
10. Gonzalez-Luque, S.; Streat, M. Uranium Sorption from Phosphoric Acid Solutions Using Selective Ion Exchange Resins. *Hydrometallurgy* **1983**, *11*, 207–225. [CrossRef]
11. Kabay, N.; Demircioğlu, M.; Yaylı, S.; Günay, E.; Yüksel, M.; Sağlam, M.; Streat, M. Recovery of Uranium from Phosphoric Acid Solutions Using Chelating Ion-Exchange Resins. *Ind. Eng. Chem. Res.* **1998**, *37*, 1983–1990. [CrossRef]
12. Kim, J.; Tsouris, C.; Mayes, R.T.; Oyola, Y.; Saito, T.; Janke, C.J.; Dai, S.; Schneider, E.; Sachde, D. Recovery of Uranium from Seawater: A Review of Current Status and Future Research Needs. *Sep. Sci. Technol.* **2013**, *48*, 367–387. [CrossRef]
13. Cao, Q.; Liu, Y.; Kong, X.; Zhou, L.; Guo, H. Synthesis of Phosphorus-Modified Poly(Styrene-Co-Divinylbenzene) Chelating Resin and Its Adsorption Properties of Uranium(VI). *J. Radioanal. Nucl. Chem.* **2013**, *298*, 1137–1147. [CrossRef]
14. Amphlett, J.T.M.; Ogden, M.D.; Foster, R.I.; Syna, N.; Soldenhoff, K.H.; Sharrad, C.A. The Effect of Contaminants on the Application of Polyamine Functionalised Ion Exchange Resins for Uranium Extraction from Sulfate Based Mining Process Waters. *Chem. Eng. J.* **2018**, *354*, 633–640. [CrossRef]
15. Zou, W.; Zhao, L.; Zhu, L. Adsorption of Uranium(VI) by Grapefruit Peel in a Fixed-Bed Column: Experiments and Prediction of Breakthrough Curves. *J. Radioanal. Nucl. Chem.* **2013**, *295*, 717–727. [CrossRef]
16. Tavakoli, H.; Sepehrian, H.; Semnani, F.; Samadfam, M. Recovery of Uranium from UCF Liquid Waste by Anion Exchange Resin CG-400: Breakthrough Curves, Elution Behavior and Modeling Studies. *Ann. Nucl. Energy* **2013**, *54*, 149–153. [CrossRef]
17. Ogden, M.D.; Moon, E.M.; Wilson, A.; Pepper, S.E. Application of Chelating Weak Base Resin Dowex M4195 to the Recovery of Uranium from Mixed Sulfate/Chloride Media. *Chem. Eng. J.* **2017**, *317*, 80–89. [CrossRef]
18. Egawa, H.; Nonaka, T.; Abe, S.; Nakayama, M. Recovery of Uranium from Seawater. X. Pore Structure and Uranium Adsorption of Macroreticular Chelating Resin Containing Amidoxime Groups. *J. Appl. Polym. Sci.* **1992**, *45*, 837–841. [CrossRef]
19. Wen, S.; Sun, Y.; Liu, R.; Chen, L.; Wang, J.; Peng, S.; Ma, C.; Yuan, Y.; Gong, W.; Wang, N. Supramolecularly Poly(Amidoxime)-Loaded Macroporous Resin for Fast Uranium Recovery from Seawater and Uranium-Containing Wastewater. *ACS Appl. Mater. Interfaces* **2021**, *13*, 3246–3258. [CrossRef] [PubMed]
20. Meng, P.; Liu, Y.; Sun, Z.; Wang, G.; Zhao, Y.; Yu, X.; Ke, P.; Li, J. Bioremediation of Low-Concentration Uranium Wastewater by Desulfovibrio Multispirans H1MTZ23 Mediated Mineralization. *Ecotoxicol. Environ. Saf.* **2026**, *313*, 119981. [CrossRef] [PubMed]
21. Amphlett, J.T.M.; Choi, S.; Parry, S.A.; Moon, E.M.; Sharrad, C.A.; Ogden, M.D. Insights on Uranium Uptake Mechanisms by Ion Exchange Resins with Chelating Functionalities: Chelation vs. Anion Exchange. *Chem. Eng. J.* **2020**, *392*, 123712. [CrossRef]
22. Stoliker, D.L.; Kaviani, N.; Kent, D.B.; Davis, J.A. Evaluating Ion Exchange Resin Efficiency and Oxidative Capacity for the Separation of Uranium(IV) and Uranium(VI). *Geochem. Trans.* **2013**, *14*, 1. [CrossRef] [PubMed]

Disclaimer/Publisher's Note: The statements, opinions and data contained in all publications are solely those of the individual author(s) and contributor(s) and not of MDPI and/or the editor(s). MDPI and/or the editor(s) disclaim responsibility for any injury to people or property resulting from any ideas, methods, instructions or products referred to in the content.